

Simulation on the relation of distribution of overall critical transport current to that of local one in bent-damaged Bi2223 superconducting composite tape

S. Ochiai,^{1,a)} M. Fujimoto,¹ H. Okuda,¹ S. S. Oh,² and D. W. Ha²

¹*Department of Materials Science and Engineering, Graduate School of Engineering, Kyoto University, Sakyo-ku, Kyoto 606-8501, Japan*

²*Korea Electrotechnology Research Institute, 28-1 Sungju-Dong, Changwon 641-120, Republic of Korea*

(Received 27 November 2008; accepted 22 January 2009; published online 23 March 2009)

The superconducting Bi2223/Ag/Ag alloy composite tape specimens with a length 6 cm, composed of a series circuit of six local elements with a length 1 cm, were bent by 0.37% and 1.0% for measurement of distributions of the overall (6 cm) and local (1 cm) critical transport current and n -value. When the damage amount was small (0.37% bending strain), the distributions of the measured local and overall critical currents were described by the three parameter Weibull distribution function, while when the damage amount was large (1.0% bending strain), those were described by the bimodal Weibull distribution function. The distributions of n -value in the diagram of n -value versus critical current for both local elements and overall specimens were expressed by the regression curve of n -value as a function of critical current and the normal distribution function for the deviation of the measured n -values from the regression curve. The experimentally measured critical current distribution and the diagram of the n -value versus critical current of the overall specimens were reproduced successfully in the computer by inputting the formulated distribution functions for the critical current and n -value of the local elements into the proposed simulation method, which used a Monte Carlo simulation method and a one-dimensional series circuit model for the generated voltage near the transition of superconducting to normal state. © 2009 American Institute of Physics. [DOI: 10.1063/1.3087782]

I. INTRODUCTION

The composite superconductor tapes are subjected to bending and tensile stresses during magnet winding and electromagnetic stress (Lorentz force) during operation.¹⁻³ In the multifilamentary Bi2223 composite tapes, the brittle Bi2223 filaments that transport superconducting current are damaged when the subjected stresses are high. Accordingly, it is needed to clarify the influence of damage evolution on the superconducting property for reliability and safe design. Until now, it has been revealed that once the applied strain exceeds the irreversible strain at which damage evolution starts, the critical current never returns to the original value even when the applied strain is released, while it returns reversibly when the applied strain is lower than the irreversible strain.¹⁻²⁶ Also it has been known that the critical current is different from position to position in a specimen and from specimen to specimen.¹⁹⁻³² Accordingly, when many specimens are tested, the local and overall critical currents are distributed, especially under the applied strain ($>$ the irreversible strain) due to the inhomogeneous damage evolution.¹⁹⁻²⁶ It is needed to reveal the statistical features of the local and overall critical transport current distributions and the relation of overall critical current distribution to local one especially under various applied strains, which are important items for reliability and safe design.

Despite the importance, the description method of the

relation of overall critical current distribution to local one has not been developed until now. If such a method be constructed, it could be a useful tool not only for description of the experimental results but also for prediction of the critical current distribution of long samples from the data of short ones. In the present work, it was attempted to develop the simulation method that enables to describe (and predict) the overall critical current distribution from the local one. For this aim, first, the distributions of the local (and overall for reference) transport critical current of the slightly and significantly bent-damaged Bi2223 composite specimens were measured experimentally and were formulated, whose details will be shown in Sec. III. Also the distribution of the n -value (referring to the sharpness of the transition from super to normal conducting state, as shown later) in the diagram of n -value versus local critical current, which was needed for the simulation, was formulated in Sec. IV. The formulated distributions of local critical current and n -value were input in the simulation method proposed in Sec. V. It will be shown that the present simulation method could successfully describe the measured overall critical current distributions.

II. EXPERIMENTAL DETAILS

As the experimental sample, the multifilamentary Bi2223/Ag/Ag alloy composite tape fabricated at Korea Electrotechnology Research Institute (KERI) was used. It contained 55 Bi2223 filaments. The thickness and width of the sample were 0.23 and 4.1 mm, respectively. The original critical currents (1 μ V/cm criterion) were 69.8, 69.5, and

^{a)}Electronic mail: shojiro.ochiai@materials.mbox.media.kyoto-u.ac.jp.

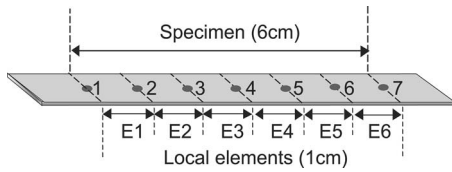


FIG. 1. Schematic representation of the test specimen with a length of 6 cm consisting of six local elements (E1–E6) with a length of 1 cm. The numbers 1–7 refer to the location of the voltage probes.

69.1 A on average for the specimen length of 1, 3, and 6 cm, respectively. The average irreversible bending strain of this sample for the critical current defined by the $1 \mu\text{V}/\text{cm}$ criterion under the specimen length of 3 cm has been estimated to be 0.25%.¹⁸

Figure 1 shows the configuration of the specimen used in the present work, in which seven voltage probes were attached in a step of 1 cm in the specimens with a length of 6 cm. Thus the present overall specimen with a length $L = 6$ cm was composed of a series circuit of the short local elements with a length of 1 cm. The specimens were bent by 0.37% and 1.0% at room temperature to cause small and large amounts of damages, respectively. [As shown later in Sec. III, the bending strains of 0.37% and 1.0% caused around 13% and 43% reductions in average critical current ($1 \mu\text{V}/\text{cm}$ criterion) of the specimens, respectively.] The specimens bent at room temperature were cooled down to 77 K at which the generated voltage (V) current (I) curves near the critical point were measured for overall specimen and local elements (E1–E6 in Fig. 1) under a self-magnetic field. The V - I curve was approximated by

$$V = AI^n, \quad (1)$$

where n and A are the fitting constants. The n -value referring to the sharpness of the transition from super to normal conducting state was estimated for the range of $V = 0.1$ to $10 \mu\text{V}/\text{cm}$ in each element and overall specimen. The critical current I_c was estimated with a criterion of $1 \mu\text{V}/\text{cm}$. As has been shown in our former work,²⁴ the critical current estimated by the $1 \mu\text{V}/\text{cm}$ criterion was not necessarily sensitive to the damages. Then, as a more damage-sensitive criterion, $1 \mu\text{V}$ criterion was also used (details will be shown in Sec. III). The critical current and n -value were measured for 96 local elements and 16 overall specimens at each bending strain (0.37% and 1.0%).

As shown later in Sec. V, the relation of n -value to critical current of local elements was needed for simulation of critical current and n -value of the overall specimens. In order to obtain the relation of local critical current to n -value for wide range of critical current, additional measurements of the n -value and critical current at $\varepsilon_B = 0\%$, 0.19%, 0.34%, 0.52%, 0.67%, and 0.83% were carried out also using the specimen shown in Fig. 1.

III. DISTRIBUTIONS OF MEASURED LOCAL AND OVERALL CRITICAL CURRENTS

The damage amount and therefore the local critical current are different from element to element. The overall specimen constitutes of the elements with different damage

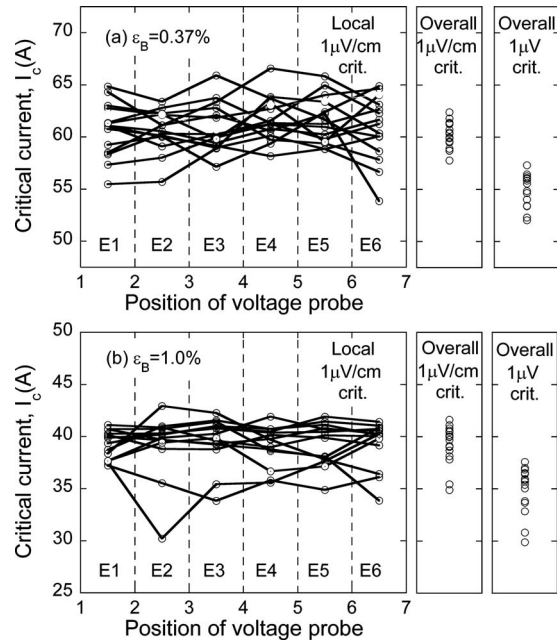


FIG. 2. Measured values of the critical current of the local elements (E1–E6) under a criterion of $1 \mu\text{V}/\text{cm}$ and overall specimens under the criteria of $1 \mu\text{V}/\text{cm}$ and $1 \mu\text{V}$ at $\varepsilon_B = 0.37\%$ and 1.0%.

amount and critical current. Accordingly, at low generated voltage, the overall critical current is more affected by the most damaged local element. If we define the overall critical current as the current at $1 \mu\text{V}$ ($1 \mu\text{V}$ criterion), the influence of the most damaged local element on the overall critical current could be incorporated. In the present work, as the criterion for the critical current, the $1 \mu\text{V}/\text{cm}$ criterion, which is used widely, and also the $1 \mu\text{V}$ one were used. The critical current of overall specimens with a length of 6 cm under the $1 \mu\text{V}/\text{cm}$ criterion, taken as the current at $V = 6 \mu\text{V}$, was higher than the critical current under the $1 \mu\text{V}$ criterion. The critical current of local elements with a length of 1 cm under the $1 \mu\text{V}/\text{cm}$ criterion was the same as that under the $1 \mu\text{V}$ one.

Figure 2 shows the measured variation in the local critical current I_c of the 1 cm elements with position of the voltage probe in the 6 cm specimens and the measured values of the overall I_c of the specimens under the $1 \mu\text{V}/\text{cm}$ and $1 \mu\text{V}$ criteria at the bending strain $\varepsilon_B = 0.37\%$ and 1.0%.

Taking the result of overall specimens as an example, the average critical currents ($1 \mu\text{V}/\text{cm}$ criterion) at $\varepsilon_B = 0.37\%$ (60.4 A) and 1.0% (39.2 A) were reduced by 13% and 43% from the original value (69.1 A), indicating that relatively small and large amounts of damages were introduced into the specimens at $\varepsilon_B = 0.37\%$ and 1.0%, respectively. As the damage amount is different from specimen to specimen, the critical current values of specimens are different to each other. The difference in damage amount among the specimens becomes larger at higher bending strain, resulting in increase in the coefficient of variation (COV) of critical current at higher bending strain.²⁶ In the present specimens, the COV at $\varepsilon_B = 0.37\%$ was 0.022 and it increased to 0.048 at $\varepsilon_B = 1.0\%$. The local ($1 \mu\text{V}/\text{cm}$ criterion) and overall ($1 \mu\text{V}$ criterion)

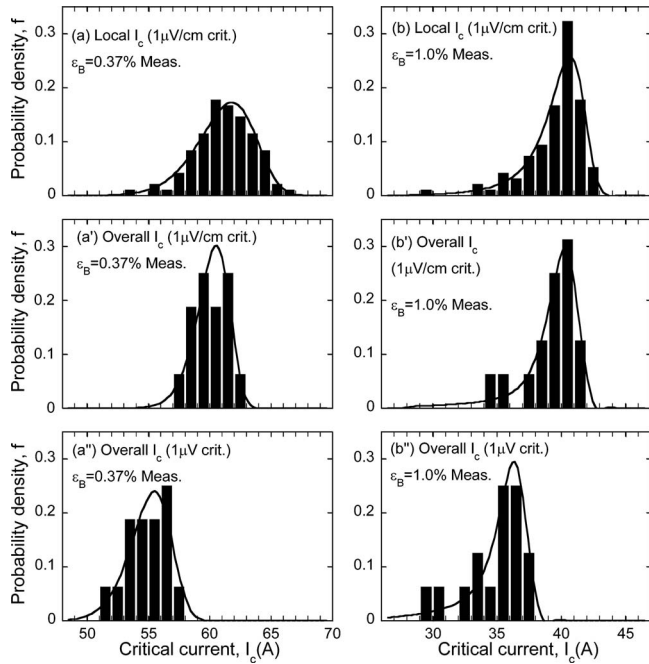


FIG. 3. Histograms of (a, b) the local critical current ($1 \mu\text{V}/\text{cm}$ criterion), (a', b') the overall critical current ($1 \mu\text{V}/\text{cm}$ criterion), and (a'', b'') the overall critical current ($1 \mu\text{V}$ criterion) at $\varepsilon_B = (a, a', a'') 0.37\%$ and (b, b', b'') 1.0% . The solid lines show the results of the regression analysis.

critical currents showed the same features as the overall critical current ($1 \mu\text{V}/\text{cm}$ criterion) mentioned above.

Figure 3 shows the histograms of (a, b) the local I_c ($1 \mu\text{V}/\text{cm}$ criterion), (a', b') the overall I_c ($1 \mu\text{V}/\text{cm}$ criterion), and (a'', b'') the overall I_c ($1 \mu\text{V}$ criterion) at $\varepsilon_B = (a, a', a'') 0.37\%$, and (b, b', b'') 1.0% . As shown in Figs. 2 and 3, the local and overall critical current values are distributed. In the present work, to describe the distribution of critical current, the Weibull distribution function,³³ which was originally proposed to describe the distribution of mechanical strength of materials, was applied due to the following reason.

The Weibull distribution has various types such as two parameter, three parameter, bimodal functions, and so on.³⁴ Concerning the applicability of the various Weibull distribution functions to the description of the critical current distribution, it has been shown that when the applied strain is low or the damage amount is small, the distribution of critical transport current can be described by the three-parameter Weibull distribution function [given by Eq. (2) below].^{23,24,32} This function has been also used to describe the critical current distribution at weak links for analysis of V - I curve under no applied strain.^{35,36} On the other hand, when the applied strain is high or the damage amount is large, it has been shown that the critical current distribution can be described by the bimodal Weibull distribution function [given by Eq. (3) later].^{24,37} The applicability of the three parameter and bimodal functions to the present experimental results (Fig. 3) was examined as follows.

The three parameter Weibull distribution function is characterized by the three parameters ($I_{c,\min}$: the minimum (lower limit) critical current below which there is no critical

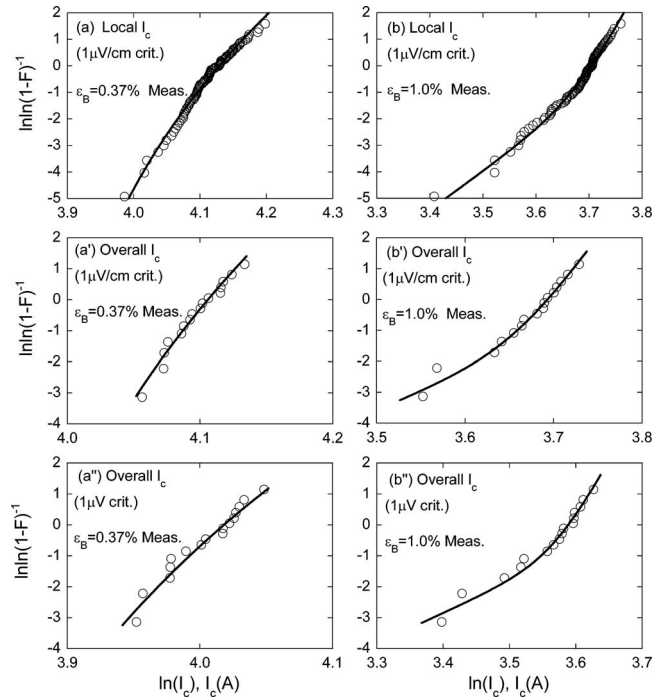


FIG. 4. Plot of $\ln \ln(1-F)^{-1}$ against $\ln(I_c)$ for (a, b) the local critical current ($1 \mu\text{V}/\text{cm}$ criterion), (a', b') the overall critical current ($1 \mu\text{V}/\text{cm}$ criterion), and (a'', b'') the overall critical current ($1 \mu\text{V}$ criterion) at $\varepsilon_B = (a, a', a'') 0.37\%$ and (b, b', b'') 1.0% . The solid lines show the results of the regression analysis.

current value, I_0 : the scale parameter, and m : the shape parameter). With these parameters, the cumulative probability F of critical current I_c is expressed by

$$F = 1 - \exp\{-[(I_c - I_{c,\min})/I_0]^m\}. \quad (2)$$

On the other hand, the bimodal Weibull distribution function is characterized by the four parameters (two shape parameters of m_1 and m_2 and two scale parameters of I_{01} and I_{02}). The cumulative probability F of this function is expressed by

$$F = 1 - \exp\{-(I_c/I_{01})^{m_1} - (I_c/I_{02})^{m_2}\}. \quad (3)$$

The features of Eqs. (2) and (3) are distinguished by the plot of $\ln \ln(1-F)^{-1}$ against $\ln(I_c)$ as follows. When $I_{c,\min} = 0$ in Eq. (2), the parameters that shall be estimated by the regression analysis are reduced to two (I_0 and m). Such a function has been called as a two parameter Weibull function. In the case of two parameter Weibull function, the relation of $\ln \ln(1-F)^{-1}$ to $\ln(I_c)$ is linear. If the measured I_c values obey the three parameter function [Eq. (2) with $I_{c,\min} > 0$], the plot of $\ln \ln(1-F)^{-1}$ against $\ln(I_c)$ deviates from the linear relation and the $\ln \ln(1-F)^{-1} - \ln(I_c)$ curve shows a convex.²⁴ In the case of bimodal function [Eq. (3)], the $\ln \ln(1-F)^{-1} - \ln(I_c)$ curve shows a concave.²⁴ Figure 4 shows the plots of $\ln \ln(1-F)^{-1}$ against $\ln(I_c)$ for (a, b) the local I_c ($1 \mu\text{V}/\text{cm}$ criterion), (a', b') the overall I_c ($1 \mu\text{V}/\text{cm}$ criterion), and (a'', b'') the overall I_c ($1 \mu\text{V}$ criterion) at $\varepsilon_B = (a, a', a'') 0.37\%$ and (b, b', b'') 1.0% . The experimental results at $\varepsilon_B = 0.37\%$ showed a convex but those at $\varepsilon_B = 1.0\%$ showed a concave, suggesting that the results at $\varepsilon_B = 0.37\%$ (a, a', a'') could be described by Eq. (2) and those at $\varepsilon_B = 1.0\%$ (b, b', b'') by Eq. (3).

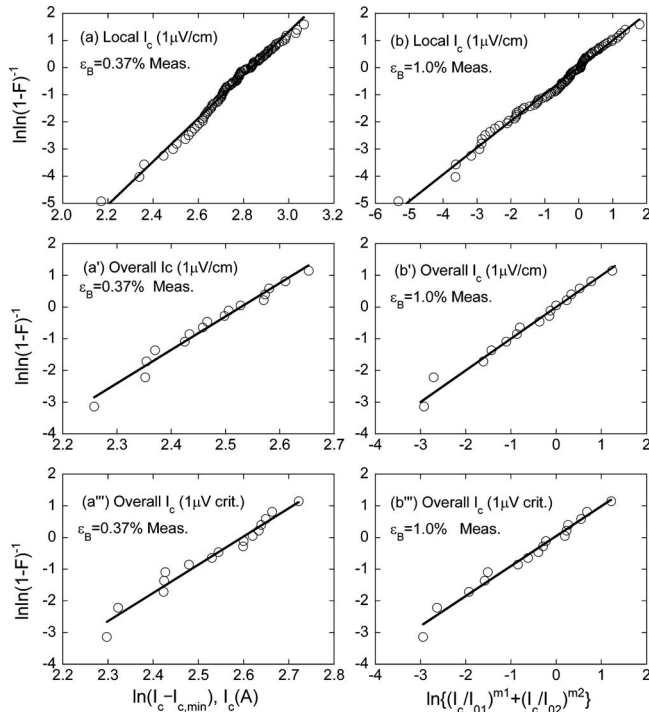


FIG. 5. High linearity (a, a', a'') in the relation of $\ln \ln(1-F)^{-1}$ to $\ln(I_c - I_{c,\min})$ at $\epsilon_B = 0.37\%$ under the estimated parameter values of $I_{c,\min}$, m , and I_0 for the three parameter distribution function [Eq. (2)] and (b, b', b'') in the relation of $\ln \ln(1-F)^{-1}$ to $\ln\{(I_c/I_{01})^{m1} + (I_c/I_{02})^{m2}\}$ under the estimated parameter values of $m1$, $m2$, I_{01} , and I_{02} for the bimodal distribution function [Eq. (3)].

The values of $I_{c,\min}$, m , and I_0 in Eq. (2) which describe the measured distributions at $\epsilon_B = 0.37\%$ [Fig. 3 (a, a', a'') and Fig. 4 (a, a', a'')] and those of $m1$, $m2$, I_{01} , and I_{02} in Eq. (3) which describe the measured distributions at $\epsilon_B = 1.0\%$ [Fig. 3 (b, b', b'') and Fig. 4 (b, b', b'')] were estimated by the regression analysis. The distributions of the local I_c (1 $\mu\text{V}/\text{cm}$ criterion), overall I_c (1 $\mu\text{V}/\text{cm}$ criterion), and overall I_c (1 μV criterion) at $\epsilon_B = 0.37\%$ were described by $(I_{c,\min}, m, I_0) = (45.1 \text{ A}, 7.98, 17.0 \text{ A})$, $(48.2 \text{ A}, 10.5, 12.5 \text{ A})$ and $(42.1 \text{ A}, 8.98, 13.6 \text{ A})$, respectively, as demonstrated by the high linearity between the $\ln \ln(1-F)^{-1}$ and $\ln(I_c - I_{c,\min})$ in Fig. 5 (a, a', a''). Those at $\epsilon_B = 1.0\%$ were described by $(m1, m2, I_{01}, I_{02}) = (37.6, 14.6, 41.1 \text{ A}, 43.5 \text{ A})$, $(40.1, 12.1, 40.5 \text{ A}, 44.7 \text{ A})$, and $(39.8, 9.81, 36.6 \text{ A}, 40.4 \text{ A})$, respectively, as demonstrated also by the high linearity between the $\ln \ln(1-F)^{-1}$ and $\ln\{(I_c/I_{01})^{m1} + (I_c/I_{02})^{m2}\}$ in Fig. 5 (b, b', b''). With these estimated values, the $\ln \ln(1-F)^{-1} - \ln(I_c)$ relations at $\epsilon_B = 0.37\%$ and 1.0% were calculated and were presented with the solid curves in Fig. 4. The experimental results were well described. Also with these values, the cumulative probability F given by Eqs. (2) and (3) was converted to the density probability f (frequency). The calculated $f-I_c$ relations at $\epsilon_B = 0.37$ and 1.0 are presented with solid curves in Fig. 3, describing well the experimental result.

The authors have been measuring the critical current distribution not only for present sample but also for other fabrication-route Bi2223-composite tape samples under various applied bending strains. In these experiments, it was found that (i) the three parameter Weibull function is appli-

cable within the applied strain range where only the tensile side is damaged, and (ii) when the compressive side is also damaged at higher applied strain, the distribution function transforms to the bimodal function. These results imply that the damage behavior is different between the tensile and compressive sides. Otto *et al.*¹⁴ reported that the buckling of the filaments occurs under compressive stress and the plural filaments are damaged at the same time by the buckling. This suggests that the damage behavior and its influence on critical current in the compressive side are different from that in the tensile side under bending.

The bimodal function [Eq. (3)] is based originally on the concept that two kinds of causes of damage act to reduce the strength of materials. As has been well known, when the two kinds of defects with different size distributions exist within the body and/or surface, the strength distribution is described by the bimodal function.³⁴ It is speculated that in a similar manner to the strength distribution, the critical current distribution is described by the bimodal function due to the coexistence of the damage both in tensile and compressive sides at high strains. Such a mechanism may be mentioned as a candidate to account for the transformation of the critical current distribution. For full understanding, further study is needed.

IV. DISTRIBUTION OF n -VALUE IN THE DIAGRAM OF n -VALUE VERSUS CRITICAL CURRENT

As will be shown later in Sec. V, the data sets of (I_c, n) of local elements are needed for simulation of distribution of I_c of overall specimens. In this subsection, the distribution of the n -value in the diagram of n -value versus critical current I_c in the local elements (and overall specimens for comparison) is formulated. The measured data sets of (I_c, n) of local elements at $\epsilon_B = 0.37\%$ (96 sets) and 1.0% (96) and at $\epsilon_B = 0\%$, 0.19% , 0.34% , 0.52% , 0.67% , and 0.83% (six sets at each bending strain) and those of overall specimens at $\epsilon_B = 0.37\%$ (16 sets) and 1.0% (16) and at $\epsilon_B = 0\%$, 0.19% , 0.34% , 0.52% , 0.67% , and 0.83% (one set at each bending strain) were used for analysis.

Figure 6(a) shows the measured n -value of each local element plotted against the corresponding I_c -value ($n-I_c$ diagram). Even for a given I_c value, the n -value is not unique, being different from element to element. The distribution of n -value in the $n-I_c$ diagram was formulated by the following two steps. In the first step, the $n-I_c$ relation was analyzed by the regression analysis. Noting the n -value that fits to the regression curve of the measured $n-I_c$ relation as n_0 , n_0 was empirically expressed as a function of I_c in the following mathematically convenient form;

$$n_0 = -295.45 + 25.692 I_c - 0.829 74 I_c^2 + 1.3043 \times 10^{-3} I_c^3 - 9.9086 \times 10^{-5} I_c^4 + 2.8944 \times 10^{-7} I_c^5. \quad (4)$$

The regression function expressed by Eq. (4) is presented with broken curves in Fig. 6(a). In the second step, in order to incorporate the distributed nature of the n -value even for a given I_c , the deviation Δn of the measured n -value from the calculated n_0 -value by Eq. (4) was estimated. The estimated

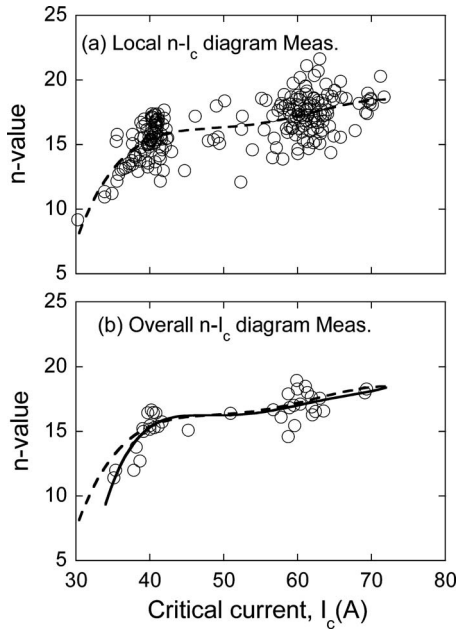


FIG. 6. Plots of the measured n -value against critical current I_c (measured n - I_c diagram) for (a) local elements and (b) overall specimens. The broken and solid lines show the results of the regression analysis of the n -value as a function of I_c for local elements [Eq. (4)] and overall specimens [Eq. (7)], respectively.

distribution of Δn is presented in Fig. 7. The standard deviation of Δn was 1.40 and the average was -0.02 . As the average was close to zero, the density distribution of Δn , $f(\Delta n)$ was approximated by the normal distribution function

$$f(\Delta n) = \frac{1}{\sigma\sqrt{2\pi}} \exp\left\{-\frac{1}{2\sigma^2}(\Delta n)^2\right\}, \quad (5)$$

where σ is the standard deviation ($=1.40$). The calculation result of Eq. (5) is presented with the solid curve in Fig. 7, describing satisfactorily the distribution of Δn . Integrating Eq. (5), we get the cumulative distribution function Δn , $F(\Delta n)$ in the form

$$F(\Delta n) = \frac{1}{\sigma\sqrt{2\pi}} \int_{-\infty}^{\Delta n} \exp\left\{-\frac{t^2}{2\sigma^2}\right\} dt. \quad (6)$$

Equation (6) with $\sigma=1.40$ will be used for simulation in Sec. V. The n - I_c diagram for the overall specimens is presented in Fig. 6(b). The regression curve of n -value as a function of I_c for the overall specimens was expressed empirically by

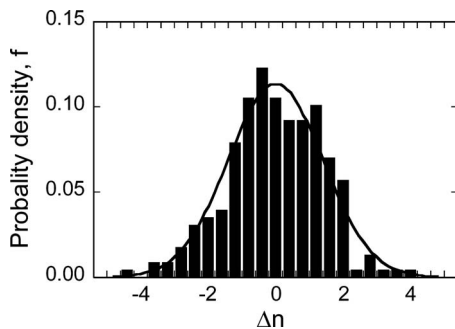


FIG. 7. Distribution of Δn value in the local elements. The solid curve shows the result of the regression analysis [Eq. (6) with $\sigma=1.40$].

$$n_0 = -892.39 + 80.759 I_c - 2.8416 I_c^2 + 4.9459 \\ \times 10^{-3} I_c^3 - 4.2589 \times 10^{-4} I_c^4 + 1.4532 \times 10^{-6} I_c^5. \quad (7)$$

The relation of n_0 to I_c given by Eq. (7) will be reproduced by the simulation in Sec. V.

V. SIMULATION OF CRITICAL CURRENT DISTRIBUTION AND DIAGRAM OF N -VALUE VERSUS CRITICAL CURRENT OF OVERALL SPECIMENS FROM THOSE OF LOCAL ELEMENTS

For prediction of the critical current distribution and the relation of n -value to critical current of bent-damaged long-length specimen from the statistical data of critical current and n -value of the short elements constituting the specimen, the following conditions shall be satisfied:

- (i) The damage evolution (and consequently the critical current and n -value) of each element constituting the overall specimen is different. Accordingly, from the statistical viewpoint, there arise the case where the damage amount is similar among the elements (the critical current and n -value of each element are rather similar in this case) and the case where the damage amount is quite different among the elements (critical current and n -value of each element are quite different from each other). If the most damaged element always determines the overall critical current, the distribution function of the extreme values (lowest critical current among the elements in each specimen) may be applicable to the prediction of the distribution of overall critical current. However, the former case cannot be treated by such a function. Both cases shall be treated comprehensively.
- (ii) The critical current of the overall specimen with a 6 cm length is defined by the current at a generated voltage of 6 μV . For prediction of the critical current and n -value of a specimen, the critical current and n -value of the six elements constituting the specimen are needed. The concrete critical current and n -values being different from element to element shall be given in advance from Eqs. (2)–(6).

As the method that satisfies these conditions, the following simulation method was used in this work. From Eq. (1), the voltage [$V(i)$] and n -value [$n(i)$] of the i -element ($i = 1-6$ in the present work) are expressed by $V(i) = A(i)I_c^{n(i)}$. For each element with a length of 1 cm, the A_i under the 1 $\mu\text{V}/\text{cm}$ criterion for determination of I_c is practically expressed by $A(i) = \{1/I_c(i)\}^{n(i)}$ ($i = 1-6$), where the $I_c(i)$ is the critical current of the i element. Thus the generated voltage of the i -element is expressed by $V(i) = \{I_c(i)\}^{n(i)}$. As the present overall specimen is composed of a one-dimensional series circuit of local elements (Fig. 1), we have the voltage of the overall specimen $V(\text{overall})$ in the form

$$V(\text{overall}) = A(\text{overall})I_c^{n(\text{overall})} = \sum \{I_c(i)\}^{n(i)}$$

$$(i = 1 - 6), \quad (8)$$

where $n(\text{overall})$ is the n -value of the overall specimen. Setting $V(\text{overall}) = 6 \mu\text{V}$ and substituting the measured values of $I_c(i)$ and $n(i)$ ($i=1-6$) of the elements constituting the specimen into Eq. (8), the overall critical current of the specimen under the $1 \mu\text{V}/\text{cm}$ criterion is calculated. The $n(\text{overall})$ value can be estimated by fitting the curve $\sum \{I_c(i)\}^{n(i)}$ to $A(\text{overall})I_c^{n(\text{overall})}$ in the range of $V = 0.6-60 \mu\text{V}$. Also the overall critical current under the $1 \mu\text{V}$ criterion can be estimated by setting $V(\text{overall}) = 1 \mu\text{V}$ in Eq. (8).

In our former works,^{23,24} it has been demonstrated that the measured overall I_c and n -value are described well by substituting the measured sets of $\{I_c(i), n(i)\}$ of the local elements into Eq. (8). Such a result means that when the sets of $\{I_c(i), n(i)\}$ ($i=1, 2, \dots, 6$) of local elements are given in advance in the simulation, the overall I_c and n -value can be calculated by Eq. (8). In the present simulation, to obtain a set of $\{I_c(\text{overall}), n(\text{overall})\}$, Eq. (8) was applied to the sets of $\{I_c(i), n(i)\}$ ($i=1-6$) which were, in advance, determined in the computer by the Monte Carlo method using random values. The simulation was carried out in a following procedure:

- (i) Determination of $I_c(i)$ of the i -local element: a random value $R(i)$ was generated in the computer. Substituting $F(i)=R(i)$ and the estimated values of $I_{c,\min} = 45.1 \text{ A}$, $m=7.98$, and $I_0=17.0 \text{ A}$ into Eq. (2), the $I_c(i)$ value of the i -element bent by 0.37% was calculated. Also substituting $F(i)=R(i)$, $m1=37.6$, $m2=14.6$, $I_{01}=41.1 \text{ A}$, and $I_{02}=43.5 \text{ A}$ into Eq. (3), the $I_c(i)$ value of the i -element bent by 1.0% was calculated.
- (ii) Determination of $n(i)$ -value of the i -local element: the $n(i)$ -value, corresponding to the $I_c(i)$ value determined in (i), was given as follows. In the first step, the $n_0(i)$ was calculated by substituting $I_c(i)$ into Eq. (4). In the second step, in order to incorporate the distributed nature of the n -value even for a given I_c , another random value $R(i)'$ was generated. Then by setting $F(\Delta n)=R(i)'$ in Eq. (6), the value of $\Delta n(i)$ was calculated. Using the $n_0(i)$ determined by the first step and $\Delta n(i)$ determined by the second step, we determined the $n(i)$ -value $\{=n_0(i)+\Delta n(i)\}$ for the i -element.
- (iii) Determination of sets of $\{I_c(i), n(i)\}$ ($i=1-6$) for one specimen: repeating the procedures (i) and (ii) for $i=1-6$, the sets of $\{I_c(i), n(i)\}$ ($i=1-6$) were determined for one specimen.
- (iv) Calculation of $\{I_c(\text{overall}), n(\text{overall})\}$ for one specimen: substituting the determined $I_c(i)$ and $n(i)$ -values ($i=1-6$) into Eq. (8), the $I_c(\text{overall})$ and $n(\text{overall})$ of one specimen were obtained.
- (v) Calculation of $\{I_c(\text{overall}), n(\text{overall})\}$ for 55 specimens to obtain distribution of $I_c(\text{overall})$ and diagram of $n(\text{overall})$ versus $I_c(\text{overall})$: The procedures (i)–

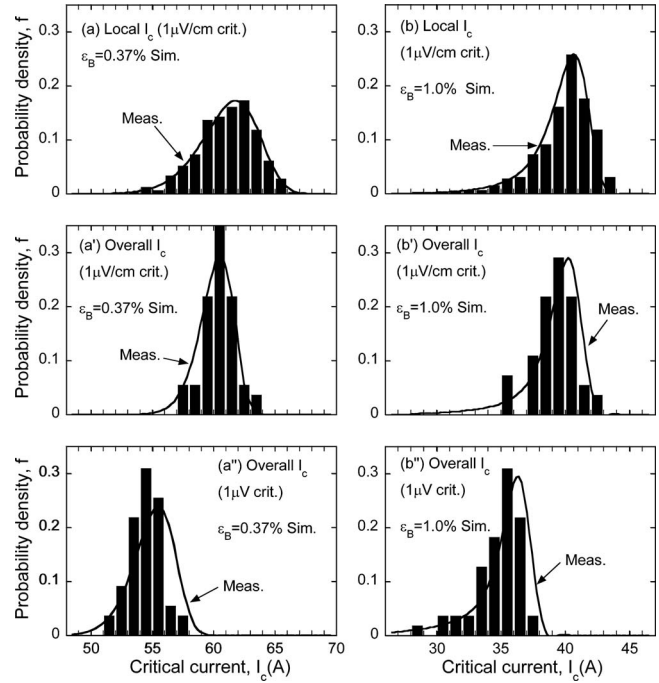


FIG. 8. Histograms of the simulated (a, b) local critical current ($1 \mu\text{V}/\text{cm}$), (a', b') overall critical current ($1 \mu\text{V}/\text{cm}$ criterion), and (a'', b'') overall critical current ($1 \mu\text{V}$ criterion) at $\varepsilon_B=(a, a', a'')$ 0.37% and (b, b', b'') 1.0%. The solid curves show the results of the regression analysis of the experimental results for comparison.

(iv) were repeated 55 times by using different random value series and the sets of $\{I_c(\text{overall}), n(\text{overall})\}$ for the 55 overall specimens were obtained for each bending strain.

By the procedure stated above, the distribution of I_c and the n - I_c diagram of the overall specimens were simulated from those of the experimental results of the local elements. Figure 8 shows the histograms of the simulated (a, b) local I_c ($1 \mu\text{V}/\text{cm}$ criterion), (a', b') overall I_c ($1 \mu\text{V}/\text{cm}$), and (a'', b'') overall I_c ($1 \mu\text{V}$) at $\varepsilon_B=(a, a', a'')$ 0.37% and (b, b', b'') 1.0%.

The solid curves show the results of the regression analysis of the experimental results taken from Fig. 3 for comparison. The experimental results are described well, indicating that the present simulation approach could be used as a first approximation for prediction of the distribution of overall critical current from the distributions of critical current and n -value of local elements.

In the experimental results within the range where the damage amount was small ($\varepsilon_B=0.37\%$), the distribution of I_c of local elements was expressed by three parameter Weibull distribution and that of overall specimen was also described by the three parameter Weibull distribution with different Weibull parameter values. Accordingly, the $\ln \ln(1-F)^{-1} - \ln(I_c)$ relation for both local and overall I_c showed a convex, as has been shown in Fig. 4 (a, a', a''). When the damage amount was large ($\varepsilon_B=1.0\%$), the distribution of I_c of local elements was expressed by the bimodal Weibull distribution and that of overall specimen was also described by the bimodal Weibull distribution with different Weibull parameter values. Accordingly, the $\ln \ln(1-F)^{-1} - \ln(I_c)$ rela-

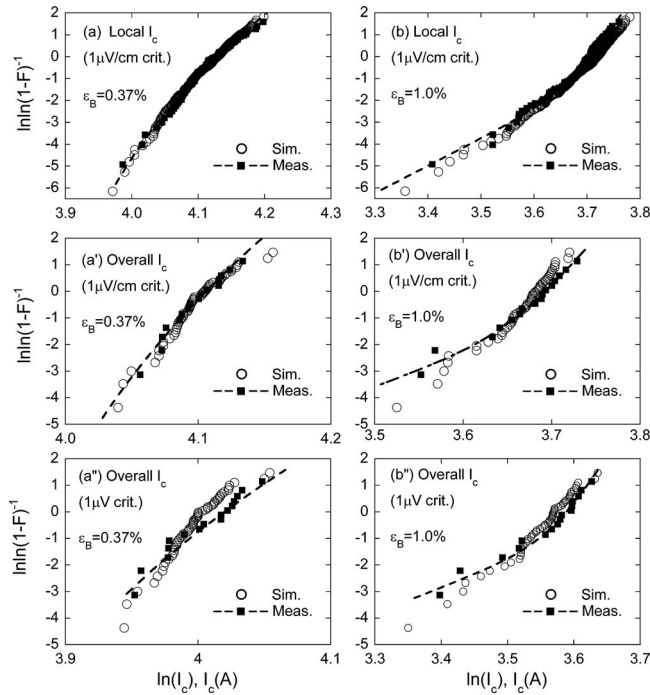


FIG. 9. Plots of $\ln \ln(1-F)^{-1}$ against $\ln(I_c)$ for the simulated (a, b) local critical current ($1 \mu\text{V}/\text{cm}$ criterion), (a', b') overall critical current ($1 \mu\text{V}/\text{cm}$ criterion), and (a'', b'') overall critical current ($1 \mu\text{V}$ criterion) at $\varepsilon_B = (a, a', a'') 0.37\%$ and (b, b', b'') 1.0% . For comparison, the measured values and their regression lines (broken curves) are presented together.

tion for both local and overall I_c showed a concave, as has been shown in Fig. 4 (b, b', b''). In order to examine whether such features are found in the simulation results or not, the relation of $\ln \ln(1-F)^{-1}$ to $\ln(I_c)$ in the simulation results was plotted in Fig. 9. The simulated $\ln \ln(1-F)^{-1} - \ln(I_c)$ relation at $\varepsilon_B = 0.37\%$ had the convex and the relation at $\varepsilon_B = 1.0\%$ had the concave, showing the same features as the experimental results.

Figure 10 shows the simulated $n-I_c$ diagram of (a) the local elements and (b) overall specimens. The broken and solid curves showed the regression curves of the experimental results given by Eqs. (4) and (7), respectively. The experimental results were well reproduced by the simulation in the whole range of the critical current investigated.

VI. CONCLUSIONS

- (1) The distributions of the measured local and overall critical current under $1 \mu\text{V}/\text{cm}$ and $1 \mu\text{V}$ criteria at $\varepsilon_B = 0.37\%$, where the damage amount was small, were described by the three parameter Weibull distribution function and those at $\varepsilon_B = 1.0\%$, where the damage amount was large, by the bimodal one. The diagram of the n -value versus critical current for local elements was expressed by the regression curve of n -value as a function of critical current in combination with the normal distribution function of the deviation Δn of the measured n -value from the regression curve.
- (2) The experimentally measured critical current distribution and the diagram of n -value versus critical current of the overall specimens were reproduced successfully from those of the local elements by means of a Monte

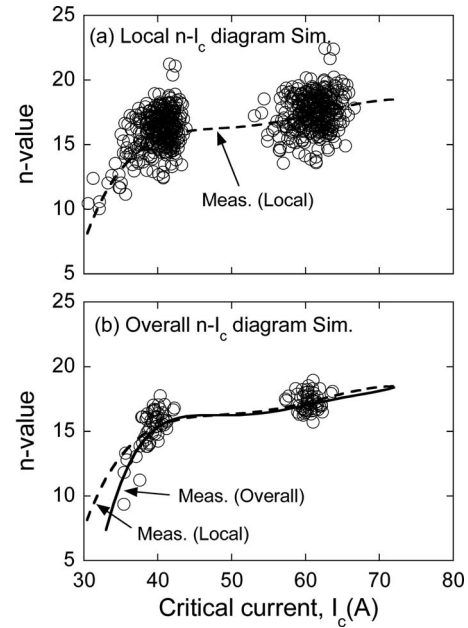


FIG. 10. Plots of the simulated n -value against the critical current I_c (simulated $n-I_c$ diagram) for (a) local elements and (b) overall specimens. The broken and solid curves show the results of regression analysis of the measured n -value as a function of measured I_c for local elements [Eq. (4)] and overall specimens [Eq. (7)], respectively, for comparison.

Carlo simulation method in combination with a one-dimensional series circuit model for the generated voltage near the transition of superconducting to normal state.

ACKNOWLEDGMENTS

The present work was supported by the grant-in-aid of the Ministry of Education, Culture, Sports, Science and Technology, Japan (Grant No.18106011).

- ¹P. Vase, R. Flükiger, M. Leghissa, and B. Glowacki, *Supercond. Sci. Technol.* **13**, R71 (2000).
- ²H. Kitaguchi, K. Itoh, H. Kumakura, T. Takeuchi, K. Togano, and W. Wada, *IEEE Trans. Appl. Supercond.* **11**, 3058 (2001).
- ³H. J. N. van Eck, K. Vargast, B. ten Haken, and H. H. J. ten Kate, *Supercond. Sci. Technol.* **15**, 1213 (2003).
- ⁴R. Wesche, A. M. Fuchs, K. Jakob, and G. Pasztor, *Cryogenics* **36**, 419 (1996).
- ⁵B. ten Haken, A. Beuink, and H. ten Kate, *IEEE Trans. Appl. Supercond.* **7**, 2034 (1997).
- ⁶R. T. Aloysius, A. Sobha, P. Guruswamy, and U. Samprasrad, *Supercond. Sci. Technol.* **14**, 85 (2001).
- ⁷R. Passerini, M. Dhallé, E. Giannini, G. Witz, B. Seeber, and R. Flükiger, *Physica C* **371**, 173 (2002).
- ⁸H. W. Weijers, J. Schwartz, and B. ten Haken, *Physica C* **372-376**, 1364 (2002).
- ⁹S. J. Sun, W. Liu, X. P. Chen, M. Y. Li, and Z. Han, *Supercond. Sci. Technol.* **16**, 984 (2003).
- ¹⁰H. J. N. van Eck, D. C. van der Laan, M. Dhallé, B. ten Haken, and H. H. J. ten Kate, *Supercond. Sci. Technol.* **16**, 1026 (2003).
- ¹¹M. Hojo, M. Nakamura, T. Matsuoka, M. Tanaka, S. Ochiai, M. Sugano, and K. Osamura, *Supercond. Sci. Technol.* **16**, 1043 (2003).
- ¹²D. C. van der Laan, H. J. N. van Eck, B. ten Haken, H. H. J. ten Kate, and J. Schwartz, *IEEE Trans. Appl. Supercond.* **13**, 3534 (2003).
- ¹³S. Ochiai, N. Miyazaki, D. Doko, T. Nagai, M. Nakamura, H. Okuda, S. S. Oh, M. Hojo, M. Tanaka, and K. Osamura, *J. Nucl. Mater.* **329-333**, 1585 (2004).

- ¹⁴A. Otto, E. J. Harley, and R. Marson, *Supercond. Sci. Technol.* **18**, S308 (2005).
- ¹⁵S. Ochiai, H. Rokkaku, K. Morishita, J. K. Shin, S. Iwamoto, H. Okuda, M. Hojo, K. Osamura, M. Sato, A. Otto, E. Harley, and A. Malozemoff, *Supercond. Sci. Technol.* **20**, 202 (2007).
- ¹⁶S. Ochiai, T. Matsuoka, J. K. Shin, H. Okuda, M. Sugano, M. Hojo, and K. Osamura, *Supercond. Sci. Technol.* **20**, 1076 (2007).
- ¹⁷S. Ochiai, H. Rokkaku, J. K. Shin, S. Iwamoto, H. Okuda, K. Osamura, M. Sato, A. Otto, and A. Malozemoff, *Supercond. Sci. Technol.* **21**, 075009 (2008).
- ¹⁸S. Ochiai, J. K. Shin, S. Iwamoto, H. Okuda, S. S. Oh, D. W. Ha, and M. Sato, *J. Appl. Phys.* **103**, 123911 (2008).
- ¹⁹S. Ochiai, T. Nagai, H. Okuda, S. S. Oh, M. Hojo, M. Tanaka, M. Sugano, and K. Osamura, *Supercond. Sci. Technol.* **16**, 988 (2003).
- ²⁰K. Katagiri, H. S. Shin, K. Kasaba, T. Tsukinokizawa, K. Hiroi, T. Kuroda, K. Itoh, and H. Wada, *Supercond. Sci. Technol.* **16**, 995 (2003).
- ²¹H. S. Shin and K. Katagiri, *Supercond. Sci. Technol.* **16**, 1012 (2003).
- ²²T. Kuroda, K. Itoh, K. Katagiri, W. Goldacker, W. Haessler, B. ten Haken, M. Kiuchi, N. Noto, S. Ochiai, S. Otabe, H. S. Shin, J. Sosnowski, H. Weijers, H. Wada, and K. Kumakura, *Physica C* **425**, 111 (2005).
- ²³S. Ochiai, D. Doko, H. Okuda, S. S. Oh, and D. W. Ha, *Supercond. Sci. Technol.* **19**, 1097 (2006).
- ²⁴S. Ochiai, M. Fujimoto, H. Okuda, S. S. Oh, and D. W. Ha, *Supercond. Sci. Technol.* **20**, 800 (2007).
- ²⁵S. Ochiai, J. K. Shin, Y. Mukai, H. Matsubayashi, H. Okuda, M. Sugano, M. Hojo, K. Osamura, T. Kuroda, K. Itoh, and H. Wada, *Physica C* **468**, 1796 (2008).
- ²⁶S. Ochiai, J. K. Shin, H. Okuda, M. Sugano, M. Hojo, K. Osamura, K. Kuroda, K. Itoh, and H. Wada, *Supercond. Sci. Technol.* **21**, 054002 (2008).
- ²⁷D. C. Larbalestier, X. Y. Cai, Y. Feng, H. Edelman, A. Umezawa, G. N. Riley, Jr., and W. L. Carter, *Physica C* **221**, 299 (1994).
- ²⁸J. Paasi, T. Kalliohaka, A. Korpela, L. Söderlund, P. F. Herman, J. Kvitkovic, and M. Majoros, *IEEE Trans. Appl. Supercond.* **9**, 1598 (1999).
- ²⁹Y. Wang, L. Xiao, L. Lin, X. Xu, Y. Lu, and Y. Teng, *Cryogenics* **43**, 71 (2003).
- ³⁰Y. Wang, S. Dai, X. Zhao, L. Xiao, L. Lin, and D. Hui, *Supercond. Sci. Technol.* **19**, 1278 (2006).
- ³¹Y. Wang, Y. Lu, X. Xu, S. Dai, D. Hui, L. Xiao, and L. Lin, *Cryogenics* **47**, 225 (2007).
- ³²A. L. Mbaruku and J. Schwarz, *J. Appl. Phys.* **101**, 073913 (2007).
- ³³W. Weibull, *ASME J. Appl. Mech.* **28**, 293 (1951).
- ³⁴Y. Matsuo, *Ceramic Engineering Handbook*, 2nd ed. (The Ceramic Society of Japan, Gihoudou, Tokyo, 2002), pp. 281–296.
- ³⁵F. Irie, Y. Tsujioka, and T. Chiba, *Supercond. Sci. Technol.* **5**, S379 (1992).
- ³⁶K. Ogawa and K. Osamura, *Physica C* **412–414**, 1124 (2004).
- ³⁷S. Ochiai, M. Fujimoto, H. Okuda, M. Sugano, M. Hojo, K. Osamura, and M. Mimura, *J. Jpn. Inst. Met.* **71**, 985 (2007).